



Published in final edited form as:

J Comp Neurol. 2014 October 15; 522(15): 3403–3422. doi:10.1002/cne.23609.

A general principle governs vision dependent dendritic patterning of retinal ganglion cells

Hong-Ping Xu^{1,*}, Jin-Hao Sun^{1,2}, and Ning Tian^{3,*}

¹Department of Neurobiology, Yale University School of Medicine, New Haven, CT, USA

²Department of Anatomy, Shandong University, School of Medicine, Jinan, Shandong, P. R. China

³Department of Ophthalmology and Visual Science, University of Utah School of Medicine, Salt Lake City, Utah, USA

Abstract

Dendritic arbors of retinal ganglion cells (RGCs) collect information over a certain area of the visual scene. The coverage territory and the arbor density of dendrites determine what fraction of visual field is sampled by a single cell and at what resolution. Yet it is not clear whether visual stimulation is required for the establishment of branching patterns of RGCs, and is there a general principle directs the dendritic patterning of diverse RGCs. By analyzing the geometric structures of RGC dendrites, we found that dendritic arbors of RGCs underwent a substantial spatial rearrangement after eye-opening. Light deprivation blocked both the dendritic growth and the branch patterning, suggesting that visual stimulation is required for the acquisition of specific branching patterns of RGCs. We further showed that vision dependent dendritic growth and arbor refinement were occurred mainly in the middle portion of the dendritic tree. This non-proportional growth and selective refinement suggested that the late-stage dendritic development of RGCs is not a passive stretching with the growth of eyes, but an active process of selective growth/elimination of dendritic arbors of RGCs driven by visual activity. Finally, our data showed that there was a power law relationship between the coverage territory and dendritic arbor density of RGCs on a cell by cell basis. RGCs are systematically less dense when they cover larger territories regardless of their cell types, retinal locations and developmental stages. These results suggest that there is a general structural design principle directs the vision dependent patterning of RGC dendrites.

*Correspondence should be addressed to: Hong-Ping Xu, 333 Cedar St, SHMB301, Department of Neurobiology, Yale University School of Medicine, New Haven, CT 06520 USA, Tel: +1 203 785 6362, Fax: +1 2037855263, hong-ping.xu@yale.edu; Ning Tian, 65 Mario Capecchi Drive, Bldg. 523, S5160 JMEC, Department of Ophthalmology and Visual Science, University of Utah School of Medicine, Salt Lake City, Utah, USA, Phone: +1 801 213-2852, Fax: +1 801 581-3357, ning.tian@hsc.utah.edu.

Associate Editor: Edward M. Callaway

Conflict of Interest Statement: There is no conflict of Interests.

Roles of Authors: Drs. Hong-Ping Xu and Ning Tian designed the experiments and wrote the manuscript. Dr. Hong-Ping Xu performed all experiments. Drs. Hong-Ping Xu and Jin-Hao Sun performed data analysis.

Keywords

retinal ganglion cell; dendritic development; visual activity; dendritic density and coverage territory; AB_10058149; AB_90755; IMSR_JAX:003782; nif-0000-10294; nif-0000-00072; rid_000069; nif-0000-30467

Introduction

Dendrites of neurons exhibit enormously diverse morphologies. The geometrical structure of dendrites is the primary determinant of neuron's biophysical property. In many cases, the size and branching pattern of dendrites can be related to neuronal functions, such as the receptive field and the number and organization of synaptic inputs (Yuste and Tank, 1996). Therefore, discovering the design principles that neurons use to configure their dendritic arbors is central to understanding how neural circuits are constructed.

The development of dendrites is a highly dynamic process of membrane extension and retraction (Cline, 1999, 2001) regulated by both intrinsic and extrinsic signals (Jan and Jan, 2003). Although genetic program is likely to determine the expression of neuronal type specific markers and the general appearance of dendritic structures, the final dendritic complexity is substantially regulated by epigenetic factors such as afferent inputs from presynaptic neurons. Blocking communications among neurons has direct consequences for the establishment of the mature dendritic morphology of neurons in many regions of the nervous system (Wong 2002), including barrel cortex pyramidal cells (Maravall et al., 2004), cerebellar Purkinje cells (Mason, et al., 1997), spinal motor neurons (Kalb, 1994), ciliary ganglia (Purves and Hume, 1981), auditory brainstem neurons (Deitch and Rubel, 1984) and retinal ganglion cells (Bodnarenko and Chalupa, 1993, Xu and Tian, 2004, 2007).

Retinal ganglion cells (RGCs) are the only output neural type of retina and relay visual signals from the eye to higher visual centers. RGCs display cell subtype specific dendritic morphologies, with over a dozen distinctive RGC subtypes performing a range of functional duties in parallel visual processing (Masland, 2001, Sun et al., 2002a; Kong et al., 2005; Coombs et al., 2006; Völgyi et al., 2009). Accumulating evidence indicated that the dendritic ramification of RGCs in different sublaminae of the inner plexiform layer (IPL) is achieved, at least partially, through vision dependent dendritic refinement (Tian and Copenhagen, 2003; Liu et al., 2007; Xu and Tian, 2007; 2008; Tian 2011; Burnat et al., 2012). However, it remains controversial whether acquisition of the coverage territory and dendritic density (the branching pattern) of RGCs requires visual stimulation. On the one hand, the adult-like morphological diversity of RGCs emerges before bipolar cells make synaptic contacts with RGCs (Diao, et al., 2004). Light deprivation had no effects on branching patterns of vast majority of RGCs that projected to either the dorsal lateral geniculate nucleus (dLGN) in cat (Lau et al., 1990, Sernagor et al., 2001) or the superior colliculus (SC) in hamster (Leventhal and Hirsch, 1983), except a small portion of RGCs with “aberrant” ipsi-lateral projections in hamster (Wingate and Thompson, 1994). These results suggested that visual experience play a limited role, if any, in the maturation of the branching pattern of RGC dendrites. On the other hand, the dendritic complexity of both alpha and beta RGCs in cat retina was found to be continuously decreased after eye-opening

(Ramoia et al., 1988; Dann et al., 1988), suggesting a dendritic remodeling occurred during the late developmental stage. It remains unclear how the branching pattern of RGC dendrites is refined after eye-opening and whether this late stage dendritic patterning requires visual stimulation. It is also not known to what extent that dendritic trees of RGCs need to be refined in order to fulfill the physiological requirement. In other words, is there a general principle that governs the activity-dependent dendritic refinement?

It has been reported that all neural arbors, both dendrites and axons, are systematically less dense when they cover larger territories (Snider et al., 2010; Teeter and Stevens, 2010). Yet it is not clear whether different subtypes of a neural population follow the same architectural design principle and whether this universal property directs the activity dependent neural arbor refinement. We sought to address these questions by examining the role of visual stimulation in the acquisition of branching patterns of RGC dendrites during development. We quantitatively examined the spatial organization of dendritic arbors and the relationship between the coverage area and the dendritic density of RGCs of different ages and rearing conditions. We found that dendritic arbors of RGCs undergo a significant spatial reorganization after eye opening. There is a non-proportional growth and selective elimination of dendritic arbors occurring after the eye-opening. Vision deprivation substantially blocked this late-stage dendritic development. We further characterized the relationship between the coverage territory and the arbor density of diverse RGC types at different ages and rearing conditions. We found that arbor densities of RGCs decrease exponentially with the increase of the coverage territory. The relationship of these two morphological features of RGCs follows one scaling law regardless of the cell types, developmental stages and rearing conditions, suggesting that a general structural design principle governs the vision dependent dendritic patterning of RGCs.

Experimental Procedures

Animals

Transgenic mice expressing Yellow Fluorescent protein (YFP, [H] line) (Feng et al., 2000, B6.Cg-Tg(Thy1-YFP)HJrs/J, RRID: IMSR_JAX:003782) in a fraction of RGCs were obtained from The Jackson Laboratory (Bar Harbor, ME). The control animals were fed and housed under 12:12-hour cyclic light/dark conditions. The average light intensity illuminating the cages during subjective days was 40 lux for control mice. Dark-reared animals were housed in conventional mouse cages, which were placed in a continuously ventilated light-tight box. The temperature and humidity inside the box were continuously monitored and controlled. All the procedures of daily monitoring and routine maintenance of dark-reared mice were conducted under infrared illumination. The handling and maintenance of animals and tissue preparation met the NIH guidelines and were approved by Yale University Committees on animal research.

Primary antibodies

Two primary antibodies were used in this study (Table 1). A polyclonal rabbit antibody against GFP (Molecular Probes, Inc., Eugene, OR, Catalog No. A21311, RRID: AB_10058149) was used to enhance fluorescent signals of YFP-expressing RGCs. This

antibody was raised against GFP isolated directly from *Aequorea Victoria* and has been characterized by immunocytochemistry in granule cells (Overstreet-Wadiche et al., 2006), olfactory sensory neurons (Levai et al., 2003), hippocampal neurons (Huang et al., 2005) and retinal ganglion cells (Xu and Tian, 2007; 2008) that express GFP or YFP. A polyclonal antibody against tyrosine hydroxylase (TH) (Chemicon AB1542, RRID: AB_90755) was used to label TH positive dopaminergic amacrine cells in the retina. This antibody was raised in sheep against pheochromocytoma tyrosine hydroxylase (Haycock and Waymire, 1982) and had been tested to stain a single band of 60 kD molecular weight in PC12 cells (manufacturer's technical information). In addition, this antibody has been used to label dopaminergic amacrine cells in the mouse retina (Xu and Tian, 2007; 2008).

Preparation of retinal whole-mounts for fluorescent imaging

The morphological assessment of RGCs were carried out on whole-mount retina preparations as described in detail previously (Xu and Tian, 2007, 2008, Xu et al., 2010). In brief, retinas with Thy1-YFP positive RGCs were isolated and fixed in 4% paraformaldehyde (PFA) in 0.01 M phosphate-buffered saline (PBS, PH 7.4) for 30 min at room temperature. Fixed retinas were washed 10 minutes in PBS for 3 times and then incubated in 30% sucrose overnight at 4 °C. After blocked in 10% normal donkey serum, retinas were incubated in a mixture of a rabbit polyclonal antibody against GFP conjugated with Alexa Fluor 488 (1:500) and a sheep polyclonal anti-TH (1:200) for 6 days at 4°C. A donkey anti-sheep secondary antibody conjugated with Texas red was used at 1:50 dilution to reveal the anti-TH bindings. Retinas were then flat mounted on Super-Frost Plus slides (Fisher Scientific, Pittsburgh, PA) with Vectashield (Vector Laboratories, Burlingame, CA) after vigorously washed 3 times in 0.01M PBS.

Confocal laser scanning microscopy

The procedure for confocal laser scanning microscopy has been described previously in detail (Xu and Tian, 2007, 2008). Briefly, fluorescent images were collected using a dual-channel Olympus FV5-PSU microscope (Optical Analysis Corporation, Nashua, NH) with a PlanApo 60x oil lens (numerical aperture: 1.4). Image stacks containing TH positive dopaminergic amacrine cells and YFP-expressing RGCs in whole mount retina were collected at z-step intervals of 0.5 µm.

Image processing and data analysis

Image J (NIH, RRID: nif-0000-30467) was used calculate pixel intensities of images. The dendritic stratification level in the inner plexiform layer (IPL) of each RGC was characterized by its peak dendritic location as described in detail before (Xu and Tian, 2007; 2008). The IPL thickness was defined as 0-100% from the border of inner nuclear layer, the best focus plane of the TH labeling dopaminergic amacrine cells, to the border of ganglion cell layer, the best focus plane of the soma of RGC. The peak dendritic location was determined by Gaussian fitting of GFP intensity in the IPL using software Igor Pro (WaveMetrics Inc. Lake Oswego, Oregon, RRID: nif-0000-00072).

Quantitative dendritic analysis of RGCs was carried out using software NeuroLucida (NeuroLucida 2000, Microbrightfield, Williston, VT, RRID: nif-0000-10294). The dendritic

field (DF) size of each RGC was measured by linking tips of dendritic arbors and the area was calculated. The dendritic density was estimated using Sholl analysis as described before (Sholl, 1953; Lau et al., 1990; Sun et al, 2002b, Xu et al., 2010). In brief, concentric circles in 25 μm equal distance apart were superimposed to each RGC with soma located at the center. The number of cross points between dendritic branches and each circle was counted (Figure 1A). The dendritic density was defined as the number of cross points per unit dendritic area. The retinal eccentricity was determined by measuring the distance from soma of the RGC to the optic nerve.

Dendritic trees of a type RGCs were then manually reconstructed using software NeuroLucida (Xu et al., 2010). Additional eight morphological parameters were measured and compared across three groups of mice with different ages and rearing conditions. These include: (i) Total dendrite length; (ii) Average dendritic length, the dendrite length per unit DF area; (iii) Branch order; (iv) Number of primary dendrites; (v) Number of dendritic ends; (vi) Segment length; (vii) Segment tortuosity, the ratio of the segment length and the straight distance between 2 nodes that define the segment. (viii) Segment planar angle, an angle between a dendritic segment and the one that it branches from computed using rays drawn from the beginning of a branch to its node or ending.

Statistical analysis

The Kolmogorov-Smirnov (K-S) test was used to determine the difference of cumulative distributions and the Student t-test was used to examine the difference between two means using software SAS 9.3 (Cary, NC, RRID: nif-0000-31484). Linear regressions were accomplished using Origin 9.1 (Northampton, MA, RRID: rid_000069). The analysis of covariance (ANCOVA) was used to compare regression slopes among groups using SAS 9.3. Data were all presented as mean \pm SEM in figures and mean \pm SD in the text.

Results

Light deprivation decreases dendritic field sizes and increases arbor densities of RGCs

Transgenic mice expressing YFP in a subset of RGCs (Feng et al., 2000; Thy1-YFP H line) were used in this study. Intense YFP signals are expressed in almost all RGC subtypes driven by Thy1 promoter as early as P12 (Xu and Tian, 2007, 2008). Figure 1A shows representative images of 11 YFP expressing RGC subtypes identified based on morphological properties described in detail previously (Masland, 2001; Sun et al., 2002; Diao et al., 2004; Xu and Tian, 2007). These RGCs ramified their dendrites in a single lamina of the inner plexiform layer (IPL) of the retina, and therefore referred to here as monostратified RGCs. We first examined the development of the branching patterns of RGCs occurring after eye-opening. The morphological properties of all 11 monostратified RGCs were characterized using Sholl analysis (Figure 1B). Individual RGCs was superimposed to 10 concentric, equidistant (25 μm) circles with soma fitted to the center. The DF was measured by linking the outermost dendritic tips and the dendritic density was estimated by counting the number of crossing points between dendritic arbors and concentric circles (Figure 1B). The DF size of YFP-expressing RGCs was significantly increased from P12 to P33 ($P < 0.001$, K-S test), suggesting a continuous growth of

dendritic arbors after eye-opening (Figure 1C). Surprisingly, the dendritic density, defined as the number of crossings in a unit DF area, was significantly reduced (Figure 1E, $P < 0.001$, K-S test), despite an increase in the total crossing number from P12 to P33 (Figure 1D, $P < 0.001$, K-S test). Light deprivation largely blocked this age-dependent DF expansion (Figure 1C, $P < 0.001$ for comparison between P33, the mice reared under normal cyclic light/dark conditions from birth to P33, and P33D, the mice reared under constant darkness from birth to P33, K-S test) and the arbor density reduction (Figure 1E, $P < 0.001$ for comparison between P33 and P33D, and $P < 0.001$ for comparison between P12 and P33D, K-S test), suggesting that visual experience plays an important role in the dendritic patterning of RGCs during the late stage development. Further studies indicated that the development of DFs and arbor densities of majority of RGC subtypes were modulated by visual experience (Table 2).

A scaling law governs the vision dependent dendritic patterning of RGCs

To understand the relationship between the DF size and the arbor density of diverse RGCs during development, we determined how the average arbor density (crossings per unit DF area) varies with the size of their territories. We found that arbors of RGCs were systematically less dense when they cover larger territories, which could be best described by a power law relationship (Figure 2A-2C, top panels). Interestingly, RGCs of the same type clustered together and clusters of different subtypes dispersed along an exponentially decreasing curve, suggesting that all RGCs follow the same scaling law regardless of their cell types (Figure 2A-C and 2F). For a better view and characterization of this relationship, we plotted arbor densities of RGCs against their DF sizes in a logarithmic space (Teeter and Stevens, 2011). The scaling exponents were characterized by computing slopes of linear regressions of these two variables in the logarithmic space (Figure 2A-C, bottom panels). There are no differences in the scaling exponents of RGCs in the P12 (slope = -0.46), P33 normal reared (slope = -0.43, $P > 0.05$ compared with the P12, ANCOVA) and P33 dark-reared animals (slope = -0.49, $P > 0.05$ compared with either the P12 or the P33, ANCOVA). These results suggested that the relationships between the DF and the arbor density of RGCs follow the same power law regardless of the cell types (Figure 2A-C and 2F) and the developmental stages (Figure 2D).

Dendrites of bistratified RGCs follow the same scaling law defined by monostratified RGCs

There is another RGC type expressing YFP intensively in the Thy1-YFP mice. The dendrites of these RGCs form two layers, the ON layer (Figure 3A) and the OFF layer (Figure 3B) arborizing in the sublamina b and a of the IPL, respectively. These bistratified RGCs respond to both the onset and the offset of light and detect moving objects at a specific direction in their receptive field. For both the ON and the OFF dendrites, the arbor density decreases when the coverage territory increases. However, the densities of these arbors were generally smaller than monostratified RGCs of similar sizes (Figure 3D and 3E, blue). Interestingly, we found that the scaling exponents (defined by slopes of linear regressions in logarithmic space) are similar for monostratified RGCs (-0.49) and bistratified RGCs (-0.44, $P > 0.05$, ANCOVA) when arbors in the ON and the OFF layers of bistratified RGCs were examined together (Figure 3C-3E, magenta), suggesting that arbors of the entire

dendritic tree of bistratified RGCs follow the same scaling law defined by monostратified RGCs (figure 3D and 3E, magenta). This power law relationship persisted from P12 to P33 and was not affected by the visual deprivation (Figure 3F), despite a substantial DF increasing and an arbor density decreasing occurred during this late developmental stage driven by visual activity (Figure 3G, 3H and Table 2).

These results suggested that the scaling law not only defines the branching patterns of RGCs of the same type, but also describes the relationship between the DF size and the arbor density of RGCs of different types and at different developmental stages.

A non-proportional growth and selective pruning of dendritic arbors of A type RGCs after eye-opening

To understand how arbor densities of RGCs are reduced at the time of their DF sizes are actively increased, we reconstructed the dendritic trees of A type RGCs at different ages and rearing conditions. Figure 4A-C shows the representative images and their reconstruction counterparts of A type RGCs collected from a P12, a P33 and a P33D mice. A type RGCs, a population homolog to the alpha cells in the rat retina (Peichl et al., 1987a, b, Sun et al., 2002b), are well conserved in their morphology throughout mammalian species (Peichl, 1991) and can be easily identified according to their large dendritic and soma sizes, 4-6 straight primary dendritic arbors and radiating branch patterning (Sun et al., 2002a; Kong et al., 2005; Coombs et al., 2006). To maintain an unbiased cell population, we analyzed all 43 A type RGCs collected from 4 retinas of P12 mice, 43 A type RGCs collected from 5 retinas of P33 mice reared under normal conditions and 40 A type RGCs collected from 5 retinas of P33 mice reared under constant darkness. The dendrites of these RGCs were clearly isolated from other YFP-expressing RGCs. On average, there was a significant increase in the DF size ($P < 0.001$, Figure 4D and table 3), as well as the total arbor length ($P < 0.001$, Figure 4E and table 3) from P12 to P33. However, the arbor density measured as the dendritic length per unit DF area was significantly decreased from P12 to P33 ($P < 0.001$, Figure 4F and table 3), which is consistent with the results obtained from the Sholl analysis (Figure 1 and table 2). We further found that the average dendritic length of A type RGCs was much less (Figure 4E), whereas the dendritic density (length per unit area) was significantly higher (Figure 4F) in retinas of the dark-reared mice than that of the normal reared ones, suggesting that visual stimulation plays an important role in the patterning of branch arbors of A type RGCs.

Since the sizes of DFs of RGCs increase with the retinal eccentricity (distance from soma of RGC to the optic nerve, Doi et al., 1995), we were wondering whether the late stage DF expansion and the dendritic arbor refinement were related to retinal locations. Our data indicated that in the mouse retina, the DFs of A type RGCs increased with the increase of retina eccentricity at P33 (Figure 4G, $r = 0.54$, $P < 0.001$ for linear regression), whereas there was no observable eccentricity-dependent increase of DFs at P12 ($r = -0.03$, $P > 0.8$ for linear regression). We also found that dendritic densities of A type RGCs decreased with the increase of retinal eccentricity in mice at the age of P33 (Figure 4H, $r = -0.72$, $P < 0.001$ for linear regression) but not P12 ($r = 0.05$, $P > 0.7$ for linear regression). Given that arbor densities of RGCs decrease with the increase of DFs (Figure 2) and that DFs decrease with

the increase of eccentricity (Figure 4G), it is not clear whether the eccentricity-dependent arbor density change (Figure 4H) was related to the DF alteration. To address this question, we grouped A type RGCs according to their retinal locations and compared their dendritic densities between the P12 and the P33 mice at similar retinal eccentricity. We found that the DFs of A type RGCs were increased (Figure 4I), but the densities of dendritic arbors were decreased (Figure 4J) from P12 to P33 for all A type RGCs regardless of their retinal eccentricity. Light deprivation substantially blocked this developmental process at all retinal locations (Figure 4G-4J). Although there was a weak linear relationship between DFs and retinal eccentricities of A type RGCs in the dark-reared mice (Figure 4G, $r = 0.43$, $P < 0.001$ for linear regression), the dendritic densities of these cells were not significantly related to retinal eccentricity (Figure 4H, $r = -0.31$, $P > 0.05$ for linear regression).

The decreasing of the dendritic density may be resulted from either the enlargement of DF or the reduction of branch number. To distinguish between these two possibilities, we characterized the dendritic geometry of A type RGCs. While the number of primary dendrites maintained at the same level (5.74 ± 1.74 at P12 and 5.58 ± 1.48 at P33, $P = 0.58$, t-test), the dendritic tips (ends) were significantly reduced from 52.74 ± 11.86 at P12 to 40.23 ± 7.28 at P33 ($P < 0.0001$, t-test, Figure 5A). These results suggested that the dendritic growth occurred after eye-opening was accompanied by a selective pruning of distal dendritic arbors. Further investigation indicated that the dendritic growth and pruning were mainly occurred at the middle portion of the dendritic tree (Figure 5B and 5C). The average arbor lengths of dendritic segments were significantly increased at branch orders of 3-5 and the numbers of dendritic arbors were decreased at orders of 5-7 from P12 to P33. Such a non-proportional increasing in the segment length and the selective clipping of the distal dendrites suggested that the maturation of dendritic tree of RGCs was not a passive stretching with the growth of the eye, but an active process with the peripheral arbors were refined more than the proximal ones. Despite the expansion of DF and the pruning of branch arbors, the segment tortuosity, the ratio of the segment length and the straight distance between 2 nodes that define the segment (Figure 5D), and the segment planar angles, an angle between a dendritic segment and the one that it branches from (Figure 5E), had limited change from P12 to P33.

To determine whether visual stimulation is required for this non-proportional growth and the selective clipping of dendritic arbors, we quantified the branching patterns of A type RGCs in mice reared under constant darkness. We found that the increase of the dendritic density was resulted from, at least partially, the retarded sculpting of distal dendritic arbors of RGCs in the dark-reared animals. A type RGCs of the dark-reared mice preserved the number of primary dendrites but increased the number of the dendritic ends (Figure 5A). The dendritic arbors of RGCs failed to be pruned at orders of 5-7 during the late developmental stage (Figure 5B) in mice reared under constant darkness. In addition, light deprivation significantly decreased the average lengths of dendritic segments at orders of 2, 3, 4 and 6 of A type RGCs (Figure 5C). Interestingly, dark rearing has little effect on the curvatures and branch angles of dendritic segments of A type RGCs (Figure 4D and 4E), and therefore, the overall appearance of these cells are similar to that of the age-matched controls reared under normal conditions.

A scaling law governs the vision dependent dendritic patterning of A type RGCs

We have showed that the arbor density of RGCs of different subtypes decreases exponentially with the increases of the DF size (Figure 2). To understand whether the relationship between these morphological features of A type RGCs follows the scaling law, we determined how the average arbor densities of A type RGCs vary with the sizes of their territories. We found a strong positive linear relationship between dendritic length and coverage territory of A type RGCs at different ages and rearing conditions (Figure 6A and Figure 6D). There are no statistical differences ($P > 0.05$, ANCOVA) of the linear regression slopes of RGCs in the P12 (slope = 0.018) and P33 mice reared under normal conditions (slope = 0.023) and P33 mice reared under constant darkness (slope = 0.02). In contrast, arbors of A type RGCs were systematically less dense when they cover larger territories. The relationship could be best described by a power law relationship (Figure 6B and 6E). For a better view and characterization of this relationship, we plotted arbor densities of A type RGCs against their DF sizes in a logarithmic space. The scaling exponents were characterized by computing slopes of linear regressions of these two variables in the logarithmic space (Figure 6C and 6F). We found that all A type RGCs follow the same exponentially decreasing function regardless of their developmental stages and rearing conditions ($P > 0.05$ for comparison of regression slopes of P12, P33 and P33D, slope = -0.71, -0.58 and -0.62, respectively, ANCOVA), suggesting a general association between the arbor density and the coverage territory of A type RGCs on a cell-by cell basis (Figure 6E and 6F).

But how dendritic density decreases with the increase of dendritic field in RGCs? It is intriguing to postulate that more dendritic arbors are eliminated when dendritic field is increased. To test this hypothesis, we plotted the number of branches and the size of dendritic field of A type RGCs and found that the branch numbers decrease exponentially with the increase of dendritic fields (Figure 6G and 6H). This result suggested that the decreasing of dendritic density during the late developmental stage was resulted from, at least partially, the reduction of branch numbers of RGCs. The number of branches of A type RGCs was not directly related to the retinal eccentricity. The slope of linear regression (Figure 6I, $r = -0.15$) between numbers of branches and retinal eccentricities of RGCs was not significantly different from zero ($P > 0.05$).

The vision dependent dendritic patterning is not related to the dendritic stratification

In mouse retina, there are two populations of A type RGCs with their dendrites ramified in either ON or OFF sublamina of the IPL (Sun et al., 2002a). RGCs undergo a visual experience dependent redistribution of dendrites from the center to specific layers of the IPL after eye-opening (Xu and Tian, 2007). We have reported that light deprivation preferentially blocked dendritic “relocation” of RGCs to the OFF sublamina (Xu and Tian, 2007) through modulation of glycine receptor mediated neurotransmission (Xu and Tian, 2008). To investigate whether the vision dependent sculpting of branching patterns of RGCs is associated with dendritic stratification, we plotted DF areas and arbor densities of RGCs against their dendritic stratification level in the IPL. The dendritic stratification of each A type RGC was determined by quantitatively measuring the peak dendritic density from the pixel intensity curve of a z-stack confocal images (Figure 6A and 6B) as described

previously (Xu and Tian, 2007; 2008). We found that the DFs were increased and the arbor densities were decreased from P12 to P33 (Figure 7C-E) for all A type RGCs regardless of their dendritic stratification level. This developmental change was partially blocked by light deprivation (Figure 6F-H), suggesting that visual activity dependent refinement of dendritic patterning was not associated with the dendritic stratification. We further grouped A type RGCs into ON and OFF subpopulations and reexamined the dendritic growth and arbor pruning occurred after eye-opening (Figure 6I-K). On average, the DF area was increased by 56% for ON RGCs ($P < 0.001$) and 87% for OFF RGCs ($P < 0.01$) and the arbor densities (crossing per unit area) was decreased by 24% ($P < 0.001$) for ON RGCs and 34% ($P < 0.001$) for OFF RGCs from P12 to P33. Light deprivation retarded the dendritic growth and branch refinement for both ON and OFF RGCs occurred after eye opening (Figure 5I-5K). The DF area was decreased by 20% for ON RGCs ($P < 0.05$) and 26% for OFF RGCs ($P < 0.01$). The arbor densities was increased by 10% for ON RGCs ($P < 0.05$) and 24% for OFF RGCs ($P < 0.01$) in P33 mice reared under constant darkness compared with that reared in the normal condition. The vision dependent arbor density reduction was accompanied by a decreasing of branch numbers. The branch points (nodes) of A type RGCs were significantly decreased from P12 to P33 and vision deprivation substantially blocked this late stage refinement of branch arbors in both the ON and the OFF A type RGCs (Figure 7K).

Discussion

We quantitatively examined the development of branching patterns of RGCs in mouse retina. We found that the acquisition of both the coverage territory and the arbor density of RGCs require visual activity. RGCs continuously increase their DF size after eye-opening by elongating branch segments in the middle portion of the dendritic tree. The expansion of the DF was accompanied by a reduction of dendritic arbor density achieved through selective elimination of branch arbors in the distal portion of the dendritic tree. Light deprivation substantially blocked both the dendritic growth and the arbor refinement. This non-proportional dendritic growth and selective elimination of dendritic arbors suggested that the late stage dendritic development of RGCs is not a passive stretching with the growth of eyes, but an active process of selective growth/elimination of dendritic arbors of RGCs driven by visual activity. Our data also showed that there was a power law relationship between the coverage territory and the arbor density of RGC dendrites on a cell by cell basis. RGCs were systematically less dense when they cover larger territories regardless of their cell types, retinal locations and developmental stages. These results suggest that there is a general structural design principle directs the visual activity dependent patterning of RGC dendrites.

Visual activity is required for both dendritic stratification and branch patterning of RGCs

There are at least a dozen morphologically distinctive RGCs subtypes in mouse retina, each playing a specific role in the parallel visual processing (Masland, 2001, Sun et al., 2002a; Kong et al., 2005; Coombs et al., 2006; Völgyi et al., 2009). The number of morphologically characterized RGC types is similar in different mammalian species, suggesting an evolutionarily conservation in the parallel channels encoding visual information. In all species that have been studied, RGCs of different subtypes arborize their dendrites in

specific layers of the IPL and receive synaptic inputs from definite presynaptic neurons. In addition, the coverage territory and the arbor density of RGCs can vary by many orders of magnitude, enabling RGCs of different subtypes sample the visual world with specific precisions. The emergence of the morphological diversity of RGCs is independent of the patterned visual stimulation (Diao et al., 2004). In mouse retina, RGCs develop from a diffusely stratified and poorly differentiated group at birth to 12 distinct, morphologically well-defined subtypes at the time of eye-opening (P13).

On the other hand, many evidences indicated that the emergence of the specific dendritic stratification of RGCs is refined by visual stimulation after eye opening. During early developmental stage, the dendritic arbors of newborn RGCs are diffusely arborized in the IPL. The diffusely stratified dendritic arbors of RGCs are gradually restricted into narrower stratum by removing of “inappropriate” dendritic arbors (Bansal et al., 2000; Bodnarenko et al., 1993, 1995; Tian and Copenhagen 2003; Xu and Tian, 2007; Tian, 2011). This initial dendritic stratification is likely driven by spontaneous retinal activity mediated by acetylcholine receptors (AChRs) as deletion of beta2 subunits of nicotinic AchRs significantly retarded the dendritic stratification of RGCs (Bansal et al., 2000). Although dendrites of most RGCs have achieved narrow ramification at the time of eye-opening (Mumm et al., 2005, Diao et al, 2004, Xu and Tian, 2007), a large majority of RGCs ramify their dendrites at the middle portion and extend their arbors into both sublamina a and b of the IPL at P10-P12 (Xu and Tian 2007; Tian and Copenhagen, 2003). These narrow-stratified RGCs likely respond to both the onset and the offset of light stimulation (Tian and Copenhagen, 2003). At the age of P33, dendritic arbors of RGCs are redistributed to different layers of the IPL and the population of ON-OFF responsive RGCs is reduced from 78% at P10-12% to 21% at the age of P27-30 (Tian and Copenhagen, 2003). Visual deprivation significantly blocked this age-dependent dendritic redistribution and the decline of ON-OFF responsive RGCs, suggesting an instructive role of visual activity in the emergence of the diverse dendritic stratification and the maturation of functional ON-OFF pathway.

The present study further suggested that the maturation of dendritic patterning is regulated by visual experience. Although gross morphologies of most majority RGCs are already shaped at the time of eye opening (Diao et al., 2004), the dendritic arbors of many subtypes are shown to bear numerous spines or filopodia, indicating an active remodeling of RGCs dendrites at this developmental stage (Wong et al., 2000; Lohmann et al., 2002, Xu et al., 2010). Similar to the development of dendritic stratification, the development of branching patterns of RGCs includes an initial increase (growth) and then a visual activity dependent decrease (refinement) of branch arbors. For instance, the complexity (reflected by branch points) of both alpha and beta RGCs in cat retina were continuously increased start from E50, reached peak around the time of eye-opening (P7-9) and then gradually decreased to adult level by eliminating of the excess branch arbors (Ramoia et al., 1988). In mouse retina, the average branch points of A type RGCs increased from < 30 at the time of birth (Diao, et al., 2004) to 46.05 ± 12.05 (mean \pm SD) at the time of eye-opening (P12) and then declined to 34.62 ± 6.9 (mean \pm SD) at P33 (the present study). Such a developmental profile of the dendritic complexity was also found in other RGC types in the mouse and the cat retina (Coombs et al., 2007; Ramoia, et al., 1988; Wingate and Thompson, 1995). Light deprivation

significantly blocked the late stage dendritic refinement, suggesting the requirement of visual experience in the branch patterning of RGCs.

While the coverage territories of RGCs was continuously increased after eye-opening, the dendritic growth was limited to branch segments in the middle of the dendritic tree, leaving arbor lengths of the most proximal and distal dendrites unchanged (Figure 2G). Similarly, although the overall dendritic complexity is reduced, only branch arbors in the middle of DF were eliminated after eye-opening (Figure 2F). Similar sensory dependent dendritic remodeling was found in dentate granule cells (Rihn and Claiborne, 1990), cerebellar purkinje cells (Weiss and Pysh, 1978) and cortical pyramidal cells (Koester and O'Leary, 1992; Maravall et al., 2004; Mizrahi and Libersat, 2002). This non-proportional dendritic growth and selective branch refinement suggested that the late stage dendritic development of RGCs is not a passive stretching with the growth of eyes, but an active process of selective growth/elimination of dendritic arbors of RGCs driven by neural activity. Consistent with this finding, it has been reported that the developmental increase of RGC DF is not proportional to the expansion of the retina diameter (Ren et al., 2009). Most RGC types exhibit a fast expansion between postnatal day 8 (P8) and P13, followed by a phase of retraction between P13 and adulthood of coverage area relative to the retina growth, suggesting the rate of DF increase of RGCs is not a direct consequence of retina growth but follows a growth pace intrinsic to the RGCs.

Dendritic stratification and patterning are regulated by visual activity through different mechanisms

There are two populations of A type RGCs in mouse retina with their dendrites stratified in either ON or OFF sublamina of the IPL. All A type RGCs that stratified in the ON sublamina exhibit sustained responses, whereas those with dendrites stratified in OFF sublamina can have either transient or sustained responses (Pang et al., 2003). The dendritic stratification of these two populations of A type RGCs is differentially modulated by visual experience. Light deprivation preferentially blocked dendritic redistribution from the center to the OFF sublamina of the IPL through modulation of glycine receptors mediated OFF synaptic transmission in the rod pathway (Xu and Tian, 2007; 2008). In contrast, the branching pattern of A type RGCs that arborized in both the ON and the OFF sublaminae of the IPL were modulated by visual experience (Figure 5), suggesting that branch patterning of RGCs was regulated by visual stimulation through mechanisms other than glycine receptor mediated neurotransmission. RGCs continuously gain arbor lengths and thus increased the DF sizes during the whole period of differentiation and development (Dann et al., 1988; Diao et al., 2004). Blocking neurotransmission in the retina reduced dendritic lengths and branch numbers of RGCs by affecting dendritic filopodia motility (Lohman et al., 2002; Wong et al., 2000; Sernagor et al., 2001, Xu et al., 2010). On the other hand, blocking spiking activity of RGCs also decreased the number of dendritic arbors of both alpha and beta RGCs in the cat retina (Wong et al., 1991). These results suggested that presynaptic inputs work in concert with postsynaptic mechanisms modulate the dendritic patterning of RGCs during development. Given that the selective dendritic refinement occurs at a time window when RGCs actively form synaptic connections with presynaptic neurons (Fisher, 1979a), it is likely that the synapse formation of RGCs plays a key role in the activity-

dependent patterning of dendritic branches (Wingate and Thompson, 1995; Wässle, 1988). Interestingly, light deprivation significantly increased the distal arbors of A type RGCs (Figure 4), as well as the conventional synapses between amacrine cells and RGCs (Sosula and Glow, 1971, Fisher, 1979b), suggesting a potential causal relationship between visual activity dependent synapse formation and the dendritic patterning.

Morphological identification of RGCs

We adopted a system of classification of RGCs used by Sun et al. in the studies of rat and mouse retinas (Sun et al., 2002a and 2002b). RGCs expressing YFP were classified into four major groups: cells with large soma and large dendritic field were classified as A type RGCs; cells with small to medium-sized soma and small to medium-sized dendritic field were classified as B type RGCs; cells with small to medium-sized soma and medium to large-sized dendritic field as C type RGCs; and cells with dendrites ramified into two layers were classified as D type RGCs. The three monostratified RGC types fall into three discrete clusters and therefore can be easily distinguished based on their overall appearance. RGCs were further categorized into subtypes based on several morphological parameters such as the stratification level and the coverage area of the dendritic field and the diameter, density and curvature of dendritic arbors. The visually identified RGCs consistently fall into one of the clusters sorted using the cluster analysis (Coombs, et al., 2006; Kong et al., 2005). For instance, the A1 and A2 subtypes are categorized as cluster 11 and 7, respectively, and the visually identified B1, B2 and B3 subtypes correspond to clusters of 2, 1, and 4, respectively (Kong et al., 2005). Although the molecular identity and the gross anatomical appearance of RGCs are dominated by genetic programs, the adult-like morphology of RGCs is acquired gradually during postnatal life and the final branching patterns of RGCs is significantly refined by neural activity. For instance, the dendritic fields of P0 RGCs display very simple to very complex branching morphologies, however, none of them are morphologically comparable to those of the adult. At the age of P13, 97% of RGCs exhibited morphological properties that can be classified into one of the adult subtypes (Diao et al., 2004). Despite many transient developmental features, such as spines and filapodia, are presented at dendritic arbors of many subtypes (Wong et al., 2000a; Lohmann et al., 2002), the gross morphologies of most majority of RGCs are already shaped at P13 (Diao et al., 2004) and the relationship between the coverage area and the arbor density of P12 RGCs follows that same scaling law as that in the adult mice. Light deprivation partially blocked the DF growth and the arbor refinement occurring during the late developmental stage, however, the overall appearances of diverse RGC types in the dark reared animals are obviously different and can be classified using the same morphological criteria. Nonetheless, our results suggested that a power law governs the activity dependent dendritic refinement independent of cell types. We propose that RGCs acquire their gross morphology through interaction of genetic factors and the spontaneous retinal activity during the early developmental stage and achieve their adult-like morphology through vision dependent refinement of branching patterns of their dendritic trees.

A scaling law governs the vision dependent dendritic patterning of all RGCs regardless of their cell type, retinal location and developmental stages

We showed that there are power law relationships between dendritic densities and coverage territories of RGCs at different ages and rearing conditions. The dendrites of all RGCs tend to be less dense when they cover larger territories. Several recent studies have found similar structural scaling relationships between the arbor densities and the coverage areas of both dendrites and axons of many neuron types in the central nervous system of various species. In 2009, Wen et al. reported a scaling law relationship between the radius and total arbor length of basal pyramidal cell dendrites (Wen et al., 2009). Further studies indicated that all of the neural arbors, both dendritic and axonal, can be described by Gaussian density functions (Snider et al., 2010) with amplitudes decrease as the arbor coverage increase (Teeter and Stevens, 2011). Our results extended previous findings by showing that: 1. The total dendritic lengths scales with the coverage sizes (Figure 6A); 2. The scaling law defined relationship between DFs and arbor densities of RGCs can be explained, at least partially, by the activity dependent elimination of dendritic arbors with the expansion of DF sizes during development; and 3. A general structural design principle defines dendritic patterning of all RGCs regardless of their cell types, retinal locations, developmental stages and rearing conditions (Figure 2D-F and Figure 6D-F). This structural association suggests that the activity-dependent refinement of dendritic arbors is governed by a general principle intrinsic to the RGC population.

The vision dependent dendritic patterning and the general structural design principle (the scaling law) can be applied to RGC of different types. In the Thy1-YFP H line, intense fluorescence proteins are expressed in almost all morphologically identified RGCs, which may create difficulties to track changes in the same categories of cells. However, we have showed that visual experience modulated dendritic patterning of bistratified RGCs following the same scaling law defined by the monostratified RGCs. The bistratified RGCs represent a unique RGC population in the retina. Their dendrites are separated into two layers and ramified into both the ON and the OFF sublaminae. This unique dendritic morphology makes the bistratified RGCs unlikely to be misidentified form other cell types. We further found that the dendritic patterning of A type RGCs, a population homolog to the alpha cells in the rat retina, also underwent significant structural remodeling driven by visual activity. Although the A type RGCs in mouse retina can be further divided into two or three categories based on their dendritic stratification (Pang et al., 2003; Manookin et al., 2010; Sun et al., 2002), our results suggested that the dendritic patterning of these cells, both the ON and the OFF population, are regulated by visual experience (Figure 7) following the general structural design principle. On the other hand, the wide expression of YFP provides us a great opportunity to examine the design principle that directs the activity-dependent dendritic patterning of the entire RGC population. Our data indicated that the dendritic patterning of almost all RGC subtypes was significantly modulated by visual activity following the general structural design principle. Although the size of dendritic field varies substantially in RGCs of different subtypes, RGCs are usually less dense when they cover larger territories regardless of their cell types (Figure 2). Light deprivation decreased the DF sizes (Figure 1C) and increased the arbor densities of majority RGC types at the age of P33 (Figure 1E, table 2). These results demonstrated that a general structural design principle

directs the vision dependent dendritic patterning of all RGCs regardless of their cell types, retinal locations, developmental stages and rearing conditions.

The morphological studies predict that mouse retina should have at least 12 physiological channels, each encoding a specific aspect of the visual scene. Yet it is not clear how RGC types based on morphological properties match to functional classes that responsible for the parallel visual processing. Although several channels (such as the direction selective RGCs) have been correlated with morphological cell types, the number of morphological RGC types generally exceeds the known physiological types (Farrow and Masland, 2011). Therefore, the physiological and the responsive properties of most of the morphological RGC types need to be determined, which will doubtlessly further our understanding of the physiological nature of the power law principle that governs the branching patterns of RGCs. On the other hand, a detailed study of the branching patterns of RGC types labeled with specific markers will also help to clarify the potential confusions of the cell type classification. By combing the physiological properties and the branching patterns of the genetically labeled RGCs, we might be able to understand the functional significance of the scaling law based patterning of dendritic arbors.

Acknowledgments

This work was supported by NIH grant R01 EY 012345, Research to Prevent Blindness (RPB), Funds from Connecticut Lion, Eye Research Foundation and a James Hudson Brown-Alexander B. Coxe fellowship from Yale University.

Literature cited

- Antibodies: “YFP was localized using a rabbit polyclonal antibody against GFP isolated directly from *Aequorea Victoria* (Molecular Probes, Cat# A21311, RRID: AB_10058149)” and “Tyrosine hydroxylase was localized using a sheep polyclonal antibody against pheochromocytoma Tyrosine hydroxylase (Chemicon Cat# AB1542, RRID: AB_90755)”
- Bansal A, Singer JH, Hwang BJ, Xu W, Beaudet A, Feller MB. Mice lacking specific nicotinic acetylcholine receptor subunits exhibit dramatically altered spontaneous activity patterns and reveal a limited role for retinal waves in forming ON and OFF circuits in the inner retina. *J Neurosci*. 2000; 20:7672–7681. [PubMed: 11027228]
- Bodnarenko SR, Chalupa LM. Stratification of ON and OFF ganglion cell dendrites depends on glutamate-mediated afferent activity in the developing retina. *Nature*. 1993; 364:144–146. [PubMed: 8100613]
- Bodnarenko SR, Jeyarasasingam G, Chalupa LM. Development and regulation of dendritic stratification in retinal ganglion cells by glutamate mediated afferent activity. *J Neurosci*. 1995; 15:7037–7045. [PubMed: 7472459]
- Bleckert A, Schwartz GW, Turner MH, Rieke F, Wong ROL. Visual space is represented by nonmatching topographies of distinct mouse retinal ganglion cell types. *Current Biology*. 2014; 24:310–315. [PubMed: 24440397]
- Burnat K, Van Der Gucht E, Waleszczyk WJ, Kossut M, Arckens L. Lack of early pattern stimulation prevents normal development of the alpha (Y) retinal ganglion cell population in the cat. *J Comp Neurol*. 2012; 520:2414–2429. [PubMed: 22237852]
- Cline, HT. Development of dendrites. In: Stuart, G.; Spruston, N.; Häusser, M., editors. *Dendrites*. New York: Oxford UP; 1999. p. 35-67.
- Cline HT. Dendritic arbor development and synaptogenesis. *Curr Opin Neurobiol*. 2001; 11:118–126. [PubMed: 11179881]

- Coombs JL, Van Der List D, Wang GY, Chalupa LM. Morphological properties of mouse retinal ganglion cells. *Neurosci.* 2006; 140:123–136.
- Coombs JL, Van Der List D, Chalupa LM. Morphological properties of mouse retinal ganglion cells during postnatal development. *J Comp Neurol.* 2007; 503:803–814. [PubMed: 17570502]
- Dann JF, Buhl EH, Peichl L. Postnatal dendritic maturation of Alpha and Beta ganglion cells in cat retina. *J Neurosci.* 1998; 8:1485–1499. [PubMed: 3367208]
- Deitch JS, Rubel EW. Afferent influences on brain stem auditory nuclei of the chicken: time course and specificity of dendritic atrophy following deafferentation. *J Comp Neurol.* 1984; 229:66–79. [PubMed: 6490976]
- Diao L, Sun W, Deng Q, He S. Development of the mouse retina: Emerging morphological diversity of the ganglion cells. *J Neurobiol.* 2004; 61:236–249. [PubMed: 15389605]
- Doi M, Uji Y, Yamamura H. Morphological classification of retinal ganglion cells in mice. *J Comp Neurol.* 1995; 356:368–386. [PubMed: 7543910]
- Farrow K, Masland RH. Physiological clustering of visual channels in the mouse retina. *J Neurophysiol.* 2011; 105:1516–1530. [PubMed: 21273316]
- Feng G, Mellor RH, Bernstein M, Keller-Peck C, Nguyen QT, Wallace M, Nerbonne JM, Lichtman JW, Sanes J. Imaging neural subsets in transgenic mice expressing multiple spectral variants of GFP. *Neuron.* 2000; 28:41–51. [PubMed: 11086982]
- Fisher LJ. Development of synaptic arrays in the inner plexiform layer of neonatal mouse retina. *J Comp Neurol.* 1979a; 187:359–372. [PubMed: 489784]
- Fisher LJ. Development of retinal synaptic arrays in the inner plexiform layer of dark-reared mice. *J Comp Neurol.* 1979b; 187:359–372. [PubMed: 489784]
- Haycock JW, Waymire JC. Activating antibodies to tyrosine hydroxylase. *J Biol Chem.* 1982; 257:9416–9423. [PubMed: 6125505]
- Huang Z, Zang K, Reichardt LF. The origin recognition core complex regulates dendrite and spine development in postmitotic neurons. *J Cell Biol.* 2005; 170:527–535. [PubMed: 16087709]
- Jan YH, Jan LY. The control of dendrite development. *Neuron.* 2003; 40:229–242. [PubMed: 14556706]
- Jakobs TC, Koizumi A, Masland RH. The spatial distribution of glutamatergic inputs to dendrites of retinal ganglion cells. *J Comp Neurol.* 2008; 510:221–236. [PubMed: 18623177]
- Kalb RG. Regulation of motor neuron dendrite growth by NMDA receptor activation. *Development.* 1994; 120:3063–3071. [PubMed: 7720552]
- Koester SE, O'Leary DDM. Functional classes of cortical projection neurons develop dendritic distinctions by class-specific sculpting of an early common pattern. *J Neurosci.* 1992; 12:1382–1393. [PubMed: 1556599]
- Kong JH, Fish DR, Rockhill RL, Masland RH. Diversity of ganglion cells in the mouse retina: Unsupervised morphological classification and its limits. *J Comp Neurol.* 2005; 489:293–310. [PubMed: 16025455]
- Lom B, Cohen-Cory S. Brain-derived neurotrophic factor differentially regulates retinal ganglion cell dendritic and axonal arborization in vivo. *J Neurosci.* 1999; 19:9928–9938. [PubMed: 10559401]
- Landi S, Cenni AC, Maffei L, Berardi N. Environmental enrichment effects on development of retinal ganglion cell dendritic stratification require retinal BDNF. *PLoS one.* 2007; 2:e346–e346. [PubMed: 17406670]
- Lau KC, So KF, Tay D. Effects of visual or light deprivation on the morphology, and the elimination of the transient features during development, of type I retinal ganglion cells in hamsters. *J Comp Neurol.* 1990; 300:583–592. [PubMed: 2273094]
- Lèvai O, Strotmann J. Projection pattern of nerve fibers from the septal organ: DiI-tracing studies with transgenic OMP mice. *Histochem Cell Biol.* 2003; 120:483–492. [PubMed: 14628145]
- Leventhal AG, Hirsch HVB. Effects of visual deprivation upon the morphology of retinal ganglion cells projecting to the dorsal lateral geniculate nucleus of the cat. *J Neurosci.* 1983; 3:332–344. [PubMed: 6185657]

- Liu X, Grishanin RN, Tolwani RJ, Rentería RC, Xu B, Reichardt LF, Copenhagen DR. Brain-derived neurotrophic factor and TrkB modulate visual experience-dependent refinement of neuronal pathways in retina. *J Neurosci*. 2007; 27:7256–7267. [PubMed: 17611278]
- Lohmann C, Myhr KL, Wong RO. Transmitter-evoked local calcium release stabilizes developing dendrites. *Nature*. 2002; 418:177–181. [PubMed: 12110889]
- Manookin MB, Weick M, Stafford BK, Demb JB. NMDA receptor contributions to visual contrast coding. *Neuron*. 2010; 67:280–293. [PubMed: 20670835]
- Maravall M, Koh IYY, Lindquist WB, Svoboda K. Experience-dependent changes in barrel dendritic branching of layer 2/3 pyramidal neurons during a critical period for developmental plasticity in rat barrel cortex. *Cerebral Cortex*. 2004; 14:655–664. [PubMed: 15054062]
- Masland RH. Neuronal diversity in the retina. *Curr Opin Neurobiol*. 2001; 11:431–436. [PubMed: 11502388]
- Mason CA, Morrison ME, Ward MS, Zhang Q, Baird DH. Axon-target interactions in the developing cerebellum. *Perspect Dev Neurol*. 1997; 5:69–82.
- Mizrahi A, Libersat F. Afferent input regulates the formation of distal dendritic branches. *J Comp Neurol*. 2002; 452:1–10. [PubMed: 12205705]
- Model Organisms: “Experiments were conducted in transgenic mouse expressing Yellow fluorescent protein in a fraction of RGCs (B6.Cg-Tg(Thy1-YFP)HJrs/J, RRID: IMSR_JAX:003782)
- Mumm JS, Godinho L, Morgan JL, Oakley DM, Schroeter EH, Wong ROL. Laminal circuit formation in the vertebrate retina. *Prog in Brain Res*. 2005; 147:155–169. [PubMed: 15581704]
- Overstreet-Wadiche LS, Bromberg DA, Bensen AL, Westbrook GL. Seizures accelerate functional integration of adult-generated granule cells. *J Neurosci*. 2006; 26:4095–4103. [PubMed: 16611826]
- Pang JJ, Gao F, Wu SM. Light-evoked excitatory and inhibitory inputs to ON and OFF α ganglion cells in the mouse retina. *J Neurosci*. 2003; 23:6063–6073. [PubMed: 12853425]
- Peichl L, Ott H, boycott BB. Alpha ganglion cells in mammalian retinae. *Proc R Soc Lond [Biol]*. 1987a; 231:169–197.
- Peichl L, Buhl EH, boycott BB. Alpha ganglion cells in the rabbit retina. *J Comp Neurol*. 1987b; 263:25–41. [PubMed: 2444630]
- Peichl L. Alpha ganglion cells in mammalian retinae: common properties, species differences, and some comments on other ganglion cells. *Vis Neurosci*. 1991; 7:155–169. [PubMed: 1931799]
- Purves D, Hume RI. The relation of postsynaptic geometry to the number of presynaptic axons that innervate autonomic ganglion cells. *J Neurosci*. 1981; 1:441–452. [PubMed: 7346563]
- Ramoia AS, Cambell G, Shatz CJ. Dendritic growth and remodeling of cat retinal ganglion cells during fetal and postnatal development. *J Neurosci*. 1988; 8:4239–4261. [PubMed: 3183722]
- Ren L, Liang H, Diao L, He S. Changing dendritic field size of mouse retinal ganglion cells in early postnatal development. *Develop Neurobiol*. 2009; 70:397–407.
- Rinn LL, Claiborne BJ. Dendritic growth and regression in rat granule cells during late postnatal development. *Developmental Brain Res*. 1990; 54:115–124.
- Sernagor E, Eglén SJ, Wong RO. Development of retinal ganglion cell structure and function. *Prog in retinal and eye Res*. 2001; 20:139–174.
- Sin WC, Haas K, Ruthazer ES, Cline HT. Dendrite growth increased by visual activity requires NMDA receptor and Rho GTPases. *Nature*. 2002; 419:475–479. [PubMed: 12368855]
- Sholl DA. Dendritic organization in the neurons of the visual and motor cortices of the cat. *J Anatomy*. 1953; 87:387–406.
- Snider J, Pillai A, Stevens CF. A universal property of axonal and dendritic arbors. *Neuron*. 2010; 66:45–56. [PubMed: 20399728]
- Sosula L, Glow PH. Increase in number of synapses in the inner plexiform layer of light deprived rat retinae: quantitative electron microscopy. *J Comp Neurol*. 1971; 141:427–452. [PubMed: 4101678]
- Sun WZ, Li N, He S. Large-scale morphological survey of mouse retinal ganglion cells. *J Comp Neurol*. 2002a; 451:115–126. [PubMed: 12209831]

- Sun WZ, Li N, He S. Large-scale morphological survey of rat retinal ganglion cells. *Visual Neurosci.* 2002b; 19:483–493.
- Teeter CM, Stevens CF. A general principle of neural arbor branch density. *Current Biol.* 2010; 21:2105–2108.
- Tian N, Copenhagen DR. Visual stimulation is required for refinement of ON and OFF pathways in postnatal retina. *Neuron.* 2003; 39:85–96. [PubMed: 12848934]
- Tian N. Developmental Mechanisms that Regulate Retinal Ganglion Cell Dendritic Morphology. *Developmental Neurobiol.* 2011; 71:1297–1309.
- Tools, Software, and Databases: “Image and data analysis were conducted with NeuroLucida V8 (<http://www.mbfioscience.com/neuroLucida>, RRID: nif-0000-10294); Igor pro V4.1 (<http://www.wavemetrics.com>, RRID: nif-0000-00072); Statistical Analysis System 9.3 (<http://www.sas.com>, RRID: nif-0000-31484); Origin 9.1 (<http://www.originlab.com>, RRID: rid_000069) and ImageJ (<http://rsb.info.nih.gov/ij/index.html>, RRID:nif-0000-30467).
- Völgyi B, Chheda S, Bloomfield SA. Tracer coupling patterns of the ganglion cell subtypes in the mouse retina. *J Comp Neurol.* 2009; 512:664–687. [PubMed: 19051243]
- Wässle H. Dendritic maturation of retinal ganglion cell. *TINS.* 1988; 11:87–89. [PubMed: 2465610]
- Weiss GM, Pysh JJ. Evidence for loss of purkinje cell dendrites during late development: a morphological Golgi analysis in the mouse. *Brain Res.* 1978; 154:219–230. [PubMed: 687992]
- Wen Q, Stepanyants A, Elston GN, Grosberg AY, Chklovskii DB. Maximization of the connectivity repertoire as a statistical principle governing the shapes of dendritic arbors. *Proc Natl Acad Sci.* 2009; 106:12536–12541. [PubMed: 19622738]
- Wingate RJT, Thompson LD. Targeting and activity-related dendritic modification in mammalian retinal ganglion cells. *J Neurosci.* 1994; 14:6621–6637. [PubMed: 7965065]
- Wingate RJT, Thompson LD. The morphological development of mammalian retinal ganglion cells. *Progress in retinal and eye research.* 1995; 14:413–435.
- Wong ROL. Differential growth and remodeling of ganglion-cell dendrites in the postnatal rabbit retina. *J Comp Neurol.* 1990; 294:109–132. [PubMed: 2324327]
- Wong ROL, Herrmann K, Shatz CJ. Remodeling of retinal ganglion cell dendrites in the absence of action potential activity. *J Neurobiol.* 1991; 22:685–697. [PubMed: 1662709]
- Wong ROL, Ghosh A. Activity-dependent regulation of dendritic growth and patterning. *Nature Review Neurosci.* 2002; 3:803–812.
- Wong WT, Faulkner-Jones BE, Sanes JR, Wong RO. Rapid dendritic remodeling in the developing retina: dependence on neurotransmission and reciprocal regulation by Rac and Rho. *J Neurosci.* 2000; 20:5024–5036. [PubMed: 10864960]
- Xu HP, Tian N. Pathway-specific maturation, visual deprivation, and development of retinal pathways. *The Neuroscientist.* 2004; 10:337–346. [PubMed: 15271261]
- Xu HP, Tian N. Retinal ganglion cell dendrites undergo a visual activity-dependent redistribution after eye opening. *J Comp Neurol.* 2007; 503:244–259. [PubMed: 17492624]
- Xu HP, Tian N. Glycine receptor-mediated synaptic transmission regulates the maturation of ganglion cell synaptic connectivity. *J Comp Neurol.* 2008; 509:53–71. [PubMed: 18425804]
- Xu HP, Chen H, Ding Q, Xie ZH, Chen L, Diao L, Wang P, Gan L, Crair M, Tian N. The Immune Protein CD3 ζ Is Required for Normal Development of Neural Circuits in the Retina. *Neuron.* 2010; 65:503–515. [PubMed: 20188655]
- Yuste R, Tank DW. Dendritic integration in mammalian neurons, a century after Cajal. *Neuron.* 1996; 116:701–716. [PubMed: 8607989]

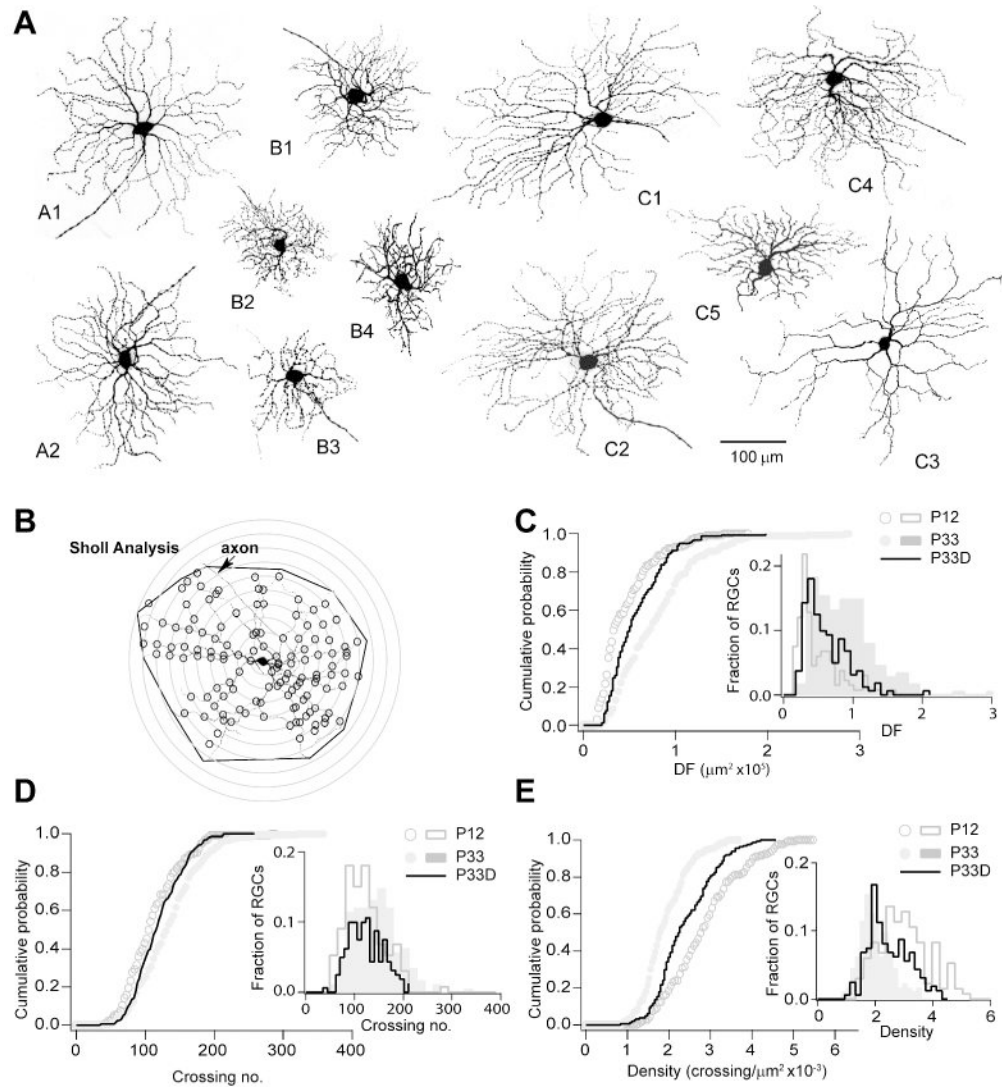


Figure 1. Sholl analysis revealed that RGCs underwent a vision dependent dendritic growth and arbor density reduction after eye-opening

(A) Representative images of diverse RGC subtypes in the retina of P33 mice. (B) Quantitative Sholl analysis of dendritic arbors of RGCs. One RGC was superimposed to 10 concentric circles with increasing radius at a 25 μm step. The outermost dendritic tips were linked to calculate dendritic field (DF) size of the RGC. The number of crossing between dendritic branches and circles was counted. Arrow points to the axon. (C) Cumulative probabilities of DF areas of monostратified RGCs collected from P12, P33 and dark-reared P33 (P33D) mice ($P < 0.001$ for comparison between P12 and P33; $P < 0.001$ for comparison between P33 and P33D; and $P < 0.001$ for comparison between P12 and P33D, K-S test). Inset, histograms of DF sizes of RGCs in the three groups of mice. (D) Cumulative probabilities of total crossing numbers of monostратified RGCs at P12, P33 and P33D mice ($P < 0.001$ for comparison between P12 and P33; $P < 0.001$ for comparison between P33 and P33D; and $P < 0.001$ for comparison between P12 and P33D, K-S test). Inset, histograms of the crossing number between concentric circles and dendritic arbors of

RGCs in the retina of P12, P33 and P33D mice. (E) Cumulative probabilities of dendritic densities of RGCs measured as number of crossing per unit DF area. Crossings at P33 mice were less dense than that at the P12 ($P < 0.001$, K-S test). Light deprivation partially blocked this developmental reduction of the dendritic arbor density ($P < 0.001$ compared with either the P12 or the P33). Inset, histograms of crossing densities of RGCs in the retina of P12, P33 and P33D mice.

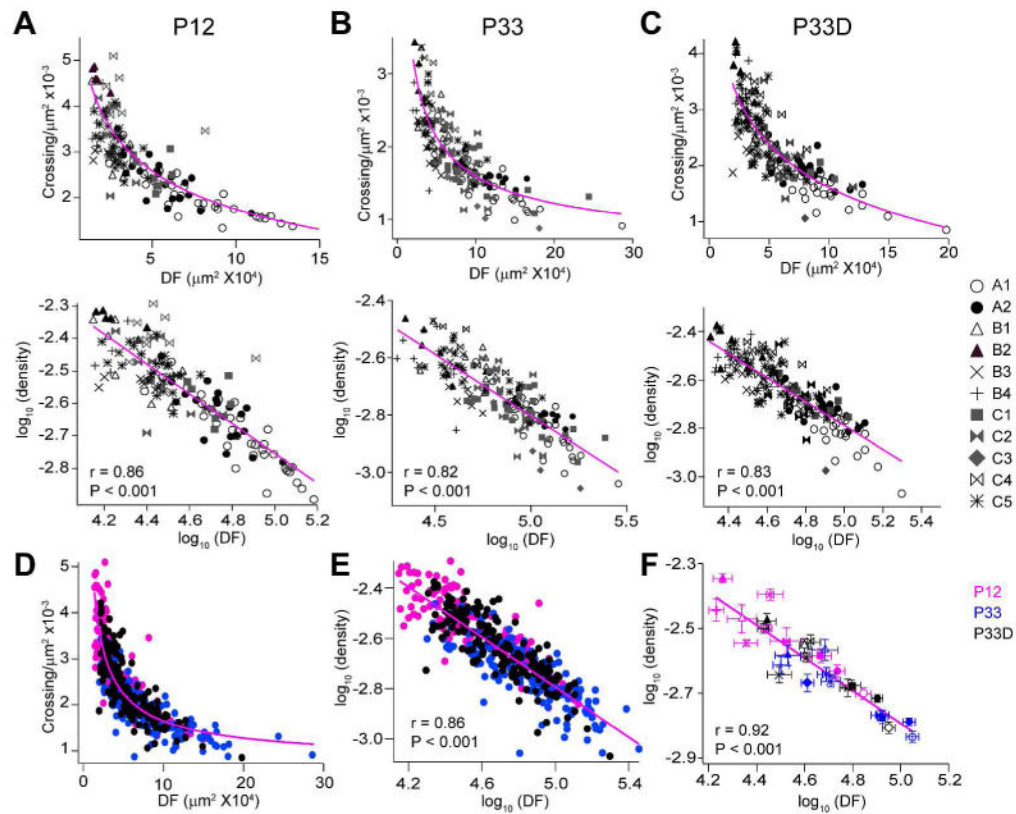


Figure 2. A general structural design principle directs the vision dependent dendritic refinement of RGCs

(A-C top) Plots of coverage areas versus dendritic densities (measured as number of crossings per unit DF area) of different RGCs types in P12 (A top), P33 (B top) and dark-reared P33 (P33D) mice (C top). Solid lines represent decreasing exponential regressions. (A-C bottom) Plots of coverage areas versus arbor densities in logarithmic spaces of diverse RGC types in P12 (A bottom), P33 (B bottom) and P33D mice (C bottom). Solid lines represent linear regressions. (D) Plots of coverage areas versus dendritic densities of RGCs in mice of different ages and rearing conditions. Solid line, decreasing exponential regression. (E) Plots of coverage areas versus dendritic densities of RGCs in mice of different ages and rearing conditions in a logarithmic space. Solid line, linear regression. (F) The coverage areas and the dendritic densities were first averaged based on cell types and then plotted in a logarithmic space. The relationship between these two morphological features follows a scaling law regardless of the cell types, developmental stages and rearing conditions.

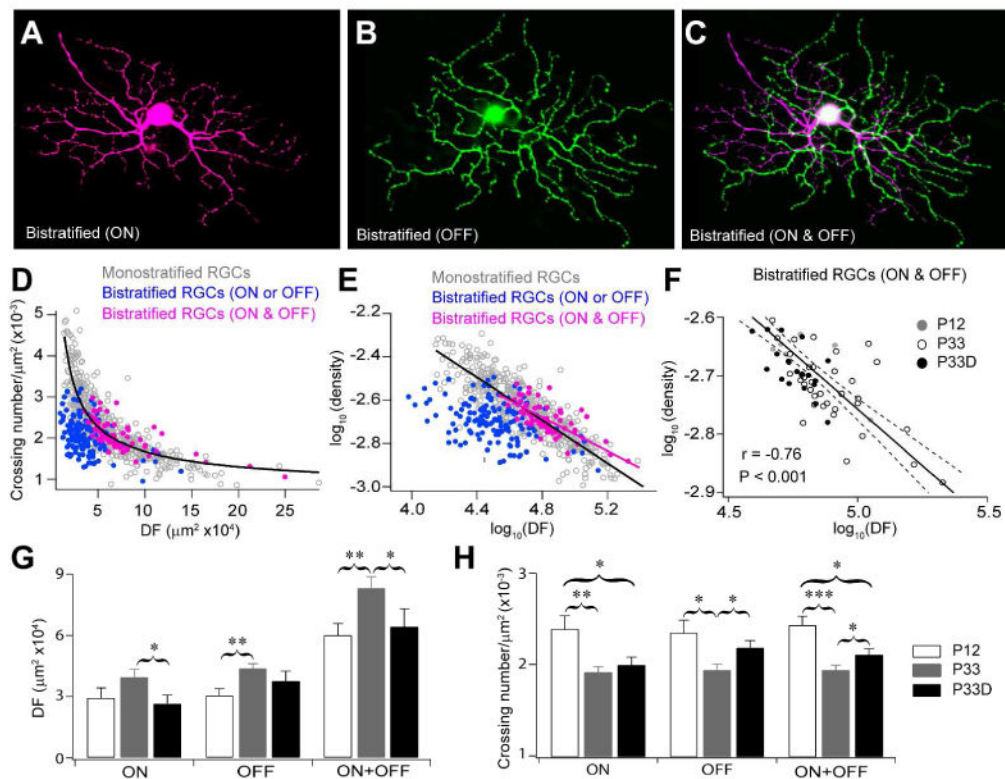


Figure 3. Dendrites of bistratified RGCs follow the same scaling law as the monostratified RGCs (A-C) Representative images of a bistratified RGC. The dendrites of this cell form two layers, the ON (A) and the OFF (B) dendritic layers, arborized in the sublamina b and a of the IPL, respectively. (C) Overlay (ON & OFF) of the two layers of dendritic arbors of the bistratified RGC. (D) Plots of the dendritic densities versus the sizes of DFs of bistratified RGCs in P12, P33 and dark-reared P33 (P33D) mice. Neither the ON nor the OFF dendrites of bistratified RGCs (ON or OFF, blue) follows the scaling law defined by monostratified RGCs. However, dendrites of bistratified RGCs and the monostratified RGCs followed the same scaling law when the ON and the OFF dendrites of bistratified RGCs were examined together (ON & OFF, magenta). (E) Plots of the dendritic densities versus the dendritic field sizes of bistratified RGCs in P12, P33 and P33D mice in a logarithmic space. There was no difference between slopes of linear regressions of monostratified RGCs (slope = -0.49) and bistratified RGCs when the ON and the OFF dendrites were examined together (magenta, slope = -0.44, $P > 0.05$, ANCOVA). (F) Plot of dendritic densities (ON & OFF) versus the dendritic field sizes (ON & OFF) of bistratified RGCs, with linear regression (solid line) and 95 % confidence interval (dashed lines). (G) The coverage areas (DF) of dendritic arbors in the ON or OFF layer and the area summation of ON and OFF arbors of bistratified RGCs in P12, P33 and P33D mice. (H) The dendritic densities (crossing/ μm^2 DF area) of dendritic arbors in the ON or the OFF layer and the density summation of ON and OFF arbors of bistratified RGCs in P12, P33 and P33D mice. *, ** and ***, $P < 0.05$, $P < 0.01$, $P < 0.001$, respectively.

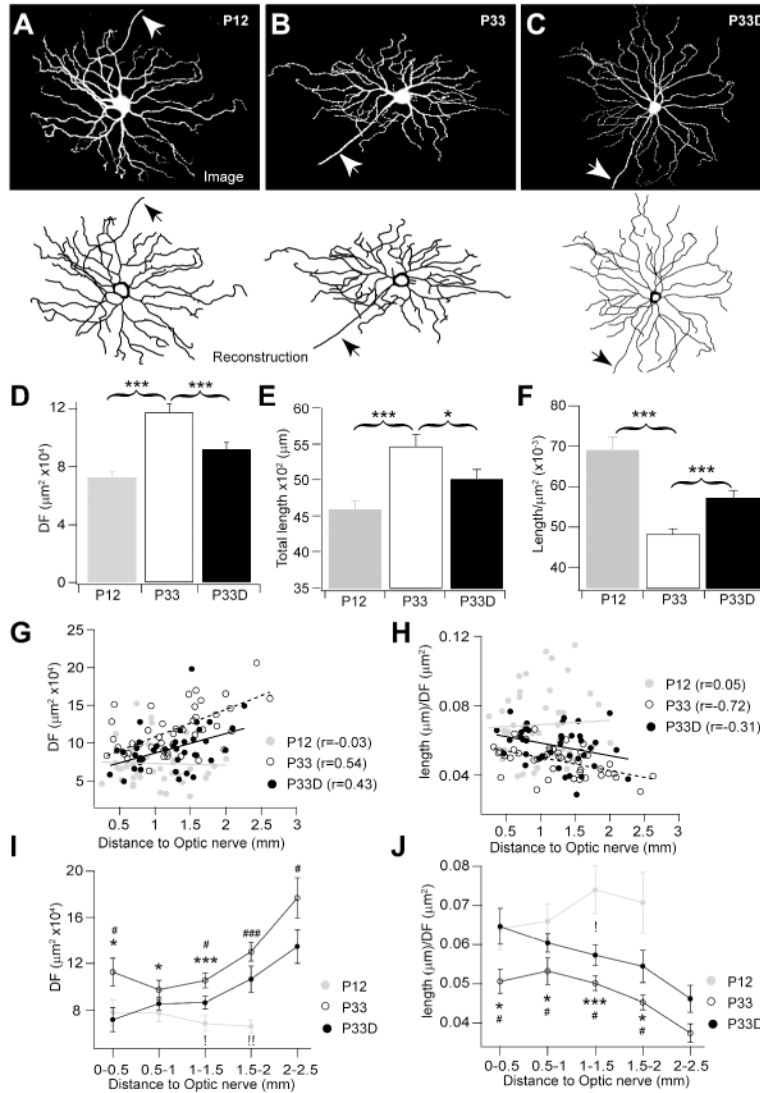


Figure 4. Light deprivation substantially blocked the dendritic growth and the arbor refinement of A type RGCs occurred after eye-opening

(A-C) Representative images (top) and their reconstruction counterparts (bottom) of A type RGCs collected from retinas of a P12 (A), a P33 (B) and a dark-reared P33 (P33D, C) mice. Arrows point to axons. (D) The sizes of dendritic fields of A type RGCs were increased from P12 to P33 ($P < 0.001$, Student t-test). Light deprivation substantially blocked this age dependent expansion of the dendritic field sizes ($P < 0.001$ for comparison between P33D and P33; $P < 0.01$ for comparison between P33D and P12, Student t-test). (E) The total arbor lengths of A type RGCs was increased from P12 to P33 ($P < 0.001$, Student t-test). Vision deprivation partially blocked the dendritic arbor growth occurred after eye-opening ($P < 0.05$ for comparison between P33 and P33D; $P < 0.05$ for comparison between P33D and P12; Student t-test). (F) The dendritic density measured as the average arbor length per unit DF area was reduced from P12 to P33 ($P < 0.001$, Student t-test). Vision deprivation partially blocked the age-dependent arbor density reduction ($P < 0.001$ for both comparisons between P33 and P33D and between P33D and P12, Student t-test). (G) Plots of DF sizes

and eccentricities of RGCs in retinas of P12, P33 and P33D mice. The DFs of A type RGCs increased with the increase of retinal eccentricity at P33 mice reared under either normal conditions ($r=0.54$, $P < 0.001$) or constant darkness ($r=0.43$, $P < 0.001$). There was no eccentricity related DF change at P12 ($r=-0.03$, $P > 0.05$). (H) Plots of dendritic arbor densities and the retinal eccentricities of RGCs in retinas of P12, P33 and P33D mice. The arbor density decreases with the increase of the retinal eccentricity at P33 mice reared under normal conditions ($r=0.72$, $P < 0.001$). There was no eccentricity related arbor density changes in P12 ($r=0.05$, $P > 0.05$) and P33D mice ($r=-0.31$, $P > 0.05$). (I) Plots of the DF sizes and the retinal locations of A type RGCs, which were grouped based on their retinal eccentricities. (J) Plots of the arbor densities and the retinal location of A type RGCs grouped based on their retinal eccentricities. *, ** and ***, $P < 0.05$, $P < 0.01$, $P < 0.001$, respectively, for comparison between P12 and P33; #, ## and ###, $P < 0.05$, $P < 0.01$, $P < 0.001$, respectively, for comparison between P33 and P33D; !, and !!, $P < 0.05$ and $P < 0.01$, respectively, for comparison between P12 and P33D for (I) and (J).

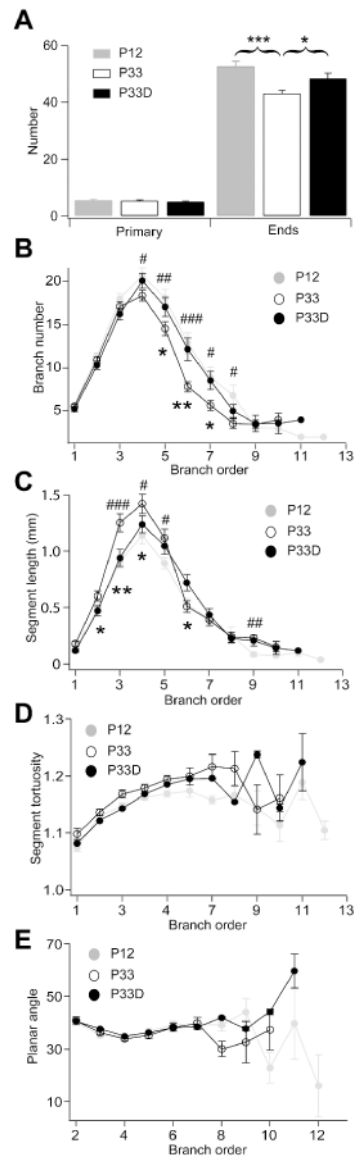


Figure 5. Dendrites of A type RGCs undergo a significant spatial reorganization after eye-opening

(A) The number of terminal dendrites (ends) in the P33 mice was significantly less than that in the P12 and the dark-reared P33 mice ($P < 0.001$; $P < 0.05$ and $P > 0.05$, for comparison between P12 and P33, comparison between P33 and P33D and comparison between P12 and P33D, respectively, Student t-test), despite the numbers of primary dendrites of A type RGCs were similar in retinas of P12, P33 and P33D mice. (B) Comparison of numbers of branches at different orders of A type RGCs in P12, P33 and P33D mice. (C) Average segment lengths of dendritic arbors at different orders of A type RGCs in the P12, P33 and P33D mice. Average segment tortuosity (D) and dendritic planar angles (E) of A type RGCs at different branch orders in the P12, P33 and P33D mice. *, ** and ***, $P < 0.05$, $P < 0.01$, $P < 0.001$, respectively, for comparison between P12 and P33; #, ## and ###, $P < 0.05$, $P < 0.01$, $P < 0.001$, respectively, for comparison between P33 and P33D.

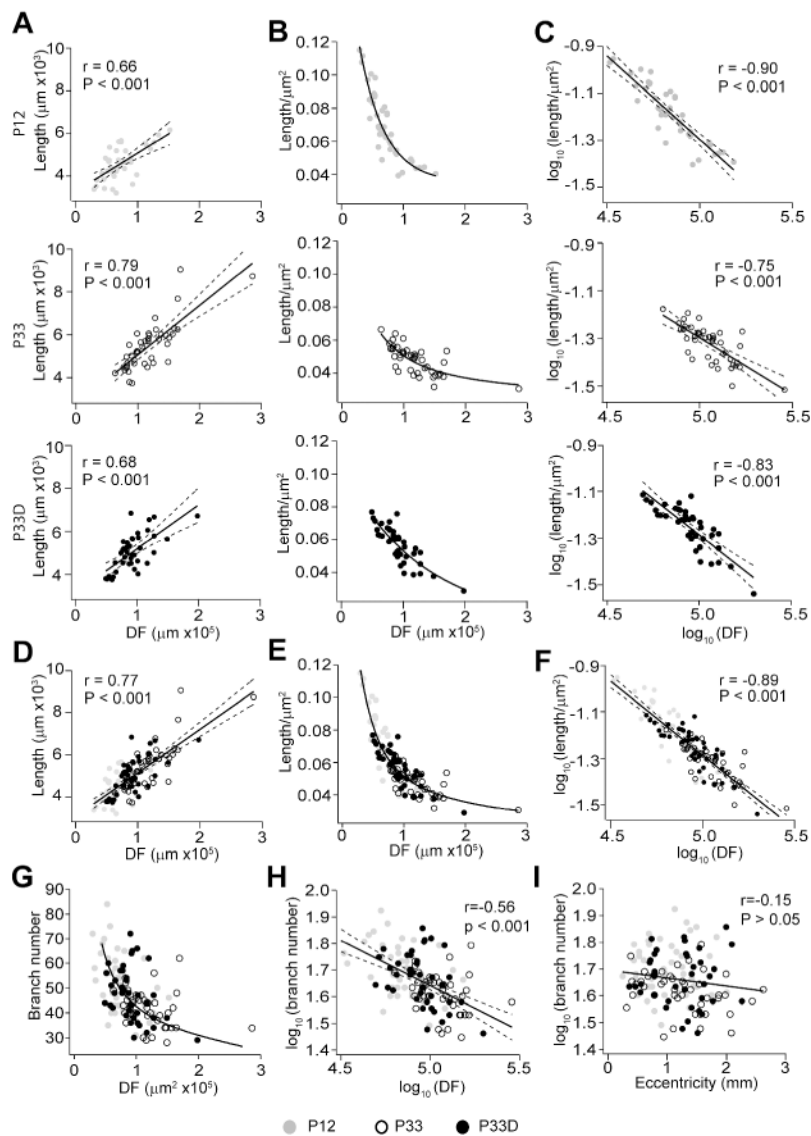


Figure 6. A scaling law describes the relationship between the coverage territory and the arbor density of A type RGCs

(A) Plots of the coverage areas versus the dendritic lengths of A type RGCs in P12 (top), P33 (middle) and dark-reared P33 (P33D, bottom) mice, with linear regressions (solid lines) and 95 % confidence intervals (dashed lines). (B) Power law relationships between the DF sizes and the arbor densities (measured by dendritic length per unit DF) of A type RGCs in P12 (top), P33 (middle) and P33D (bottom) mice. (C) Plots of coverage areas versus arbor densities in logarithmic spaces of A type RGCs in P12 (top), P33 (middle) and P33D (bottom) mice, with linear regressions (solid lines) and 95 % confidence intervals (dashed lines). (D-F) Plots of dendritic length (D) and dendritic density (E) versus DF size of all A type RGCs collected from three groups (P12, P33 and P33D) of mice. Solid and dashed lines in D represent linear regressions and 95 % confidence intervals, respectively. Solid line in E represents the exponentially decreasing regression. (F) Plots of dendritic densities versus the DF sizes of A type RGCs from all three groups of mice in a logarithmic space, with linear

regressions (solid lines) and 95 % confidence intervals (dashed lines). (G) Plots of the branch numbers versus the DF areas of A type RGCs in P12, P33 and P33D mice, with exponentially decreasing regressions (solid line). (H) Plots of branch numbers versus the DF areas of A type RGCs in P12, P33 and P33D mice in a logarithmic space, with linear regression (solid lines) and 95 % confidence interval (dashed lines). (I) Plots of branch numbers and the retinal eccentricities of A type RGCs in the three groups of mice.

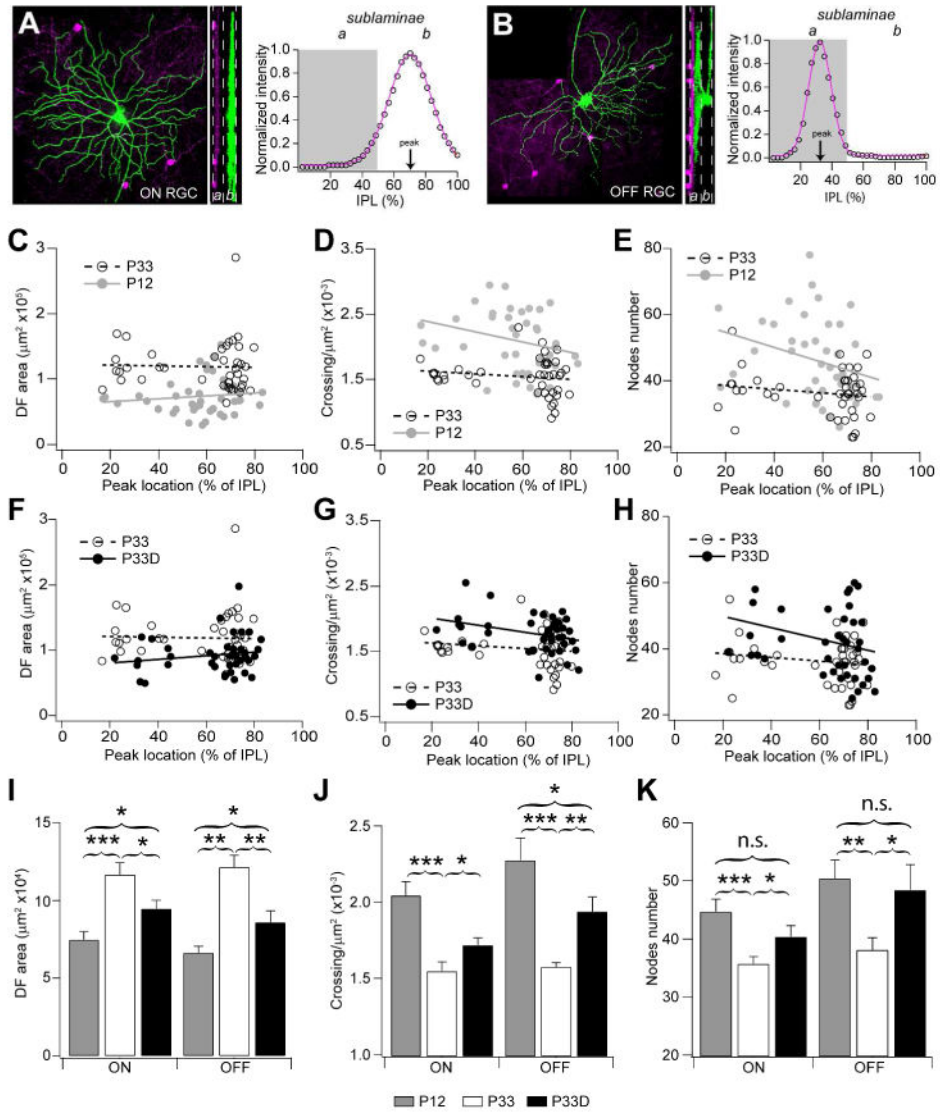


Figure 7. Visual activity dependent dendritic growth and patterning of RGCs was not related to their dendritic stratification

(A) A Representative ON A type RGC and its dendritic stratification in the IPL. Left, maximum X-Y projection of an image stack showing the branching pattern of the RGC (green) and TH positive dopaminergic amacrine cells (magenta). Middle, Y-Z projection of the same image stack showing dendritic stratification of the RGC. Right, Gaussian fitting of pixel intensity curve of the image stack. The pixel intensity of this RGC peaked (arrow) at 72 % of the IPL. The shadowed area indicates sublamina a. (B) A Representative OFF A type RGC in X-Y (left) and Y-Z (middle) projections. Right, the pixel intensity of this OFF RGC peaked (arrow) at 31 % of the IPL measured by Gaussian fitting of the pixel intensity curve. The DF area (C) and the dendritic density measured by either the Sholl analysis (D, crossing) or dendritic reconstruction (E, nodes) of RGCs in P12 and P33 mice were plotted against the peak dendritic location in the IPL. (F-H) Scatter plots of the DF area (F) and the dendritic density measured by either the Sholl analysis (G) or the dendritic reconstruction

(H) as a function of peak dendritic locations of RGCs from mice reared under either normal condition (P33) or constant darkness (P33D). (I) Average DF area of ON and OFF A type RGCs of P12 mice reared under normal condition and P33 mice reared under either normal or dark condition. (J) Average dendritic density of ON and OFF A type RGCs of P12 mice reared under normal condition and P33 mice reared under either normal or dark condition. (K) Average nodes number of ON and OFF A type RGCs of P12 mice reared under normal condition and P33 mice reared under either normal or dark condition. *, ** and ***, $P < 0.05$, $P < 0.01$, $P < 0.001$, respectively; n.s., not statistically different.

Table 1
Primary Antibodies

Antibody	Immunogen	Manufacturer	Host
anti-GFP	GFP isolated directly from <i>Aequorea Victoria</i> characterized by immunostaining in granule cells ³⁷ , olfactory sensory neurons ²⁷ , hippocampal neurons ¹⁸ and RGCs ⁶⁶⁻⁶⁷	Molecular Probes, Inc., Eugene, OR, Catalog No. A21311, RRID: AB_10058149	Rabbit polyclonal
anti-TH	Pheochromocytoma tyrosine hydroxylase characterized by immunostaining of TH neurons in retina ⁶⁶⁻⁶⁷ and western blotting of PC12 cells (single 60 KD band)	Chemicon, Catalog No. AB1542 RRID: AB_90755	Sheep polyclonal

Table 2
Dendritic fields (DFs) and arbor densities of RGCs based on Sholl analysis

Cell type	Ages	Cell number (%)	DF ($\mu\text{m}^2 \times 10^4$)	Crossing number (Sholl analysis)	Density (crossing/ $\mu\text{m}^2 \times 10^{-3}$)
A1	P12	34 (22.97)	7.65 ± 0.32 [!]	143.1 ± 32.7	2.04 ± 0.51 ^{!!!}
	P33	32 (15.17)	11.88 ± 4.45 ^{****}	166.66 ± 32.05 ^{**}	1.50 ± 0.33 ^{****}
	P33D	26 (14.13)	9.35 ± 3.17 [#]	141.46 ± 25.28 ^{##}	1.59 ± 0.30
A2	P12	20 (13.51)	5.71 ± 1.87 ^{!!!}	129.7 ± 27.6 ^{!!}	2.4 ± 0.50 ^{!!!}
	P33	18 (8.53)	11.14 ± 2.66 ^{****}	178.89 ± 31.67 ^{****}	1.64 ± 0.20 ^{****}
	P33D	21 (11.41)	8.22 ± 2.00 ^{###}	156.62 ± 29.49 [#]	1.94 ± 0.24 ^{###}
B1	P12	8 (5.41)	2.32 ± 0.88 ^{!!}	75.71 ± 20.36 ^{!!}	3.48 ± 0.90
	P33	13 (6.16)	5.11 ± 1.43 ^{***}	115.15 ± 27 ^{**}	2.31 ± 0.43 [*]
	P33D	7 (3.80)	3.99 ± 0.47 [#]	112.00 ± 19.27	2.81 ± 0.38 [*]
B2	P12	7 (4.73)	1.85 ± 0.46 ^{!!}	82.67 ± 14.12	4.52 ± 0.35 ^{!!!}
	P33	7 (5.69)	3.55 ± 1.21 ^{**}	90.14 ± 19.56	2.65 ± 0.51 ^{****}
	P33D	9 (4.89)	2.85 ± 0.78	93.44 ± 17.41	3.36 ± 0.56 [*]
B3	P12	7 (4.72)	2.35 ± 0.67	66.43 ± 16.02	2.85 ± 0.16 ^{!!}
	P33	12 (5.69)	4.17 ± 0.82 ^{***}	88.92 ± 14.32 [*]	2.20 ± 0.51 ^{**}
	P33D	8 (4.35)	3.28 ± 1.20	74.13 ± 21.30	2.31 ± 0.38
B4	P12	3 (2.032)	1.72 ± 0.37 ^{!!!}	64 ± 22.43	3.64 ± 0.75
	P33	13 (6.16)	3.27 ± 0.82 ^{***}	79.85 ± 20.54	2.49 ± 0.50 [*]
	P33D	13 (7.07)	2.72 ± 0.53	86.69 ± 20.19	3.18 ± 0.40 ^{###}
C1	P12	8 (5.41)	4.80 ± 1.20 [!]	124.5 ± 32.5	2.63 ± 0.36 ^{!!!}
	P33	26 (12.32)	9.07 ± 4.7 ^{****}	148.54 ± 54.55	1.74 ± 0.29 ^{****}
	P33D	12 (6.52)	6.51 ± 2.01 [#]	135.25 ± 31.36	2.13 ± 0.27 ^{###}
C2	P12	11 (7.43)	3.88 ± 2.80 [!]	101.82 ± 35.95	3.01 ± 0.87 ^{!!}
	P33	24 (11.37)	8.60 ± 1.93 ^{****}	143.42 ± 25.71 [*]	1.73 ± 0.40 ^{****}
	P33D	13 (7.07)	6.24 ± 2.00 [#]	128.31 ± 33.48	2.12 ± 0.52 [#]

Cell type	Ages	Cell number (%)	DF ($\mu\text{m}^2 \times 10^4$)	Crossing number (Sholl analysis)	Density (crossing/ $\mu\text{m}^2 \times 10^{-3}$)
C3	P12	0 (0)	-	-	-
	P33	4 (1.89)	11.47 ± 4.88	112.5 ± 42.54	0.99 ± 0.15
	P33D	1 (0.54)	8.01	85	1.06
C4	P12	10 (6.76)	3.13 ± 1.79	124.2 ± 59.56	4.05 ± 0.53 !!!
	P33	5 (2.37)	5.00 ± 1.48 *	132.60 ± 22.05	2.74 ± 0.45 ***
	P33D	12 (6.52)	4.43 ± 1.58	124.58 ± 32.86	2.91 ± 0.51
C5	P12	27 (18.24)	2.86 ± 0.75 !!!	89.37 ± 19.17 !!	3.19 ± 0.44 !!!
	P33	21 (9.95)	5.59 ± 2.54 ***	116 ± 36.92 **	2.20 ± 0.38 ***
	P33D	39 (21.19)	4.29 ± 1.55 #	106.95 ± 25.24	2.64 ± 0.58 ###
D (on)	P12	13 (8.78)	2.95 ± 1.72	68.85 ± 35.91	2.39 ± 0.51 !
	P33	36 (17.06)	3.94 ± 2.38	73.31 ± 40.02	1.91 ± 0.36 **
	P33D	23 (12.5)	2.67 ± 1.98 #	49.43 ± 26.46	2.00 ± 0.41
D (off)	P12	13	3.07 ± 1.15	72.62 ± 33.48	2.35 ± 0.49
	P33	36	4.37 ± 1.40 **	81.97 ± 20.77	1.94 ± 0.37 *
	P33D	23	3.75 ± 2.32	76.48 ± 24.73	2.18 ± 0.37 #
D (on+off)	P12	13	6.02 ± 2.01	141.46 ± 29.65	2.43 ± 0.35 !
	P33	36	8.31 ± 3.43 **	155.28 ± 46.17	1.94 ± 0.31 ***
	P33D	23	6.41 ± 4.22 #	125.91 ± 46.50 #	2.11 ± 0.33 #

* P < 0.05 for comparison between P12 and P33

** P < 0.01 for comparison between P12 and P33

*** P < 0.001 for comparison between P12 and P33

P < 0.05 for comparison between P33 and P33D

P < 0.01 for comparison between P33 and P33D

P < 0.001 for comparison between P33 and P33D

! P < 0.05 for comparison between P12 and P33D

!! P < 0.01 for comparison between P12 and P33D

P < 0.001 for comparison between P12 and P33D

NIH-PA Author Manuscript

NIH-PA Author Manuscript

NIH-PA Author Manuscript

Table 3
Quantification of the dendritic structure of A type RGCs

	P12	P33	P33D
Dendritic length (μm)	4587 \pm 749 [!]	5468 \pm 1121 ^{***}	5002 \pm 821 [#]
DF area (μm^2)	7.65 \pm 0.32 ^{!!}	11.88 \pm 4.45 ^{***}	9.35 \pm 3.17 ^{###}
Dendritic density ($\mu\text{m}/\mu\text{m}^2$)	0.069 \pm 0.003 ^{!!!}	0.049 \pm 0.009 ^{***}	0.056 \pm 0.011 ^{###}
Total nodes	46.05 \pm 12.06	36.42 \pm 6.90 ^{***}	42.4 \pm 11.66 ^{##}
Number of primary dendrites	5.74 \pm 1.24	5.58 \pm 1.48	5.23 \pm 1.62
Number of dendritic ends	52.74 \pm 11.86	43.23 \pm 2.78 ^{***}	48.5 \pm 11.84 [#]
Number of branch segments	98.6 \pm 24.07	79.76 \pm 13.77 ^{***}	90.75 \pm 23.36 ^{##}

* P < 0.05 for comparason between P12 and P33

** P < 0.01 for comparason between P12 and P33

*** P < 0.001 for comparason between P12 and P33

P < 0.05 for comparason between P33 and P33D

P < 0.01 for comparason between P33 and P33D

P < 0.001 for comparason between P33 and P33D

[!] P < 0.05 for comparason between P12 and P33D

^{!!} P < 0.01 for comparason between P12 and P33D

^{!!!} P < 0.001 for comparason between P12 and P33D